

**Circadian profiling in two mouse models of lysosomal storage disorders;
Niemann Pick type-C and Sandhoff disease**

Katie Richardson^{a+}, Achilleas Livieratos^{a+}, Richard Dumbill^a, Steven Hughes^b,
Gauri Ang^a, David A. Smith^c, Lauren Morris^c, Laurence A. Brown^b, Stuart N.
Peirson^b, Frances M. Platt^c, Kay E. Davies^{a*} and Peter L. Oliver^{a*}

^aMedical Research Council Functional Genomics Unit, Department of Physiology, Anatomy and Genetics, University of Oxford, Parks Road, Oxford, OX1 3PT, UK.

^bNuffield Department of Ophthalmology, Nuffield Department of Clinical Neurosciences, University of Oxford, West Wing, John Radcliffe Hospital, UK.

^cDepartment of Pharmacology, University of Oxford, Mansfield Road, Oxford, UK.

⁺these authors contributed equally to the work

*Co-corresponding authors:

email: kay.davies@dpag.ox.ac.uk tel: +44 (0)1865 285880

email: peter.oliver@dpag.ox.ac.uk tel: +44 (0)1865 285861 (submitting author)

Abstract

Sleep and circadian rhythm disruption is frequently associated with neurodegenerative disease, yet it is unclear how the specific pathology in these disorders leads to abnormal rest/activity profiles. To investigate whether the pathological features of lysosomal storage disorders (LSDs) influence the core molecular clock or the circadian behavioural abnormalities reported in some patients, we examined mouse models of Niemann-Pick Type-C (*Npc1* mutant, *Npc1^{nih}*) and Sandhoff (*Hexb* knockout, *Hexb^{-/-}*) disease using wheel-running activity measurement, neuropathology and clock gene expression analysis. Both mutants exhibited regular, entrained rest/activity patterns under light:dark (LD) conditions despite the onset of their respective neurodegenerative phenotypes. A slightly shortened free-running period and changes in *Per1* gene expression were observed in *Hexb^{-/-}* mice under constant dark conditions (DD); however, no overt neuropathology was detected in the suprachiasmatic nucleus (SCN). Conversely, despite extensive cholesterol accumulation in the SCN of *Npc1^{nih}* mutants, no circadian disruption was observed under constant conditions. Our results indicate the accumulation of specific metabolites in LSDs may differentially contribute to circadian deregulation at the molecular and behavioural level.

Keywords

lysosome storage disorder; ataxia; mouse mutant; circadian

1. Introduction

Lysosomal storage disorders (LSDs) constitute a large group of inherited metabolic diseases that typically involve pathology in the central nervous system [1, 2]. Defects in acidic hydrolases, lysosomal membrane proteins or non-enzymatic soluble lysosomal proteins underlie the majority of LSDs, often resulting in the accumulation of incompletely metabolised macromolecules inside organelles of the endosomal–autophagic–lysosomal system [3,4]. For example, mutations in genes encoding the proteins deficient in Niemann-Pick disease, type-C1 (*NPC1*) or type-C2 (*NPC2*) lead to severe neurodegeneration and liver dysfunction [5-7]. In addition, Sandhoff disease is a related LSD that arises from mutations in the β -subunit of the lysosomal enzyme β -hexosaminidase (*HEXB*) with a resultant accumulation of GM2 gangliosides in the endolysosomal compartment and severe neuronal degeneration [2]. Both these disorders are typical amongst LSDs in that the neurological symptoms are a major feature of the disease [8], including ataxia, motor deterioration and cognitive defects [2].

Circadian rhythm disruption is frequently observed in neurological disorders and it is becoming apparent that sleep disturbance is a potentially important prodromal symptom in neurodegenerative disease [9-11]; for example, rapid eye movement sleep behaviour disorder (RBD) is present years before the diagnosis of Parkinson's disease in up to 50% of patients [12,13]. Similar observations have been documented in LSDs, including patients with juvenile neuronal ceroid lipofuscinosis and Sanfilippo syndrome, where sleep disruption including irregular sleep/wake patterns are commonly reported [14-16]. With particular relevance this study, sleep

disruption has been described as a characteristic of patients with infantile and juvenile GM2 gangliosidosis [17,18]. Furthermore, in Niemann-Pick disease, cataplectic attacks have been associated with excessive daytime sleepiness [19], in addition to altered sleep efficiency and reduced sleep time - including REM and delta sleep - compared to age-matched controls [20]. A more recent study has identified restless and disturbed sleep in both infantile and adult onset NPC1 patients; however, sleep problems are often over-looked and under-reported which in part may be attributed to the severe course of the disease [21]. Indeed, emerging evidence highlights the link between the circadian clock and metabolic pathways [22, 23]; however, it is unclear whether the cellular defects associated with metabolic disorders such as LSDs influence directly the core molecular clock and thus sleep/wake activity and timing.

In order to investigate whether the specific pathologies related to the LSDs NPC and Sandhoff disease influence circadian behaviour, we examined mouse models of both these disorders, the *Npc1* null mutant (*Npc1^{nih}*) and *Hexb* knockout (*Hexb^{-/-}*) [24,25]. For the first time, rest/activity profiles were assessed in these mutants using wheel-running activity measurement in addition to neuropathological and clock gene expression analysis. Interestingly, our data suggests that individual cellular pathways affected in LSDs may contribute to some aspects of circadian deregulation at the behavioural and molecular level.

2. Materials and methods

2.1 Mice

Npc1^{nih} (BALB/cNctr-*Npc1^{m1N}*) mutant mice contain a retroposon insertion leading to a complete absence of the protein in homozygous animals [25]. Mutants show some subtle motor-coordination defects at 7-8 weeks of age, followed by progressive ataxia from 9 weeks, before reaching disease end-stage at 10-12 weeks [26,27]. *Hexb^{-/-}* mutant mice were originally generated by introduction of a neomycin-resistant vector disrupting exon 2 of the gene [24]; these mice show impaired motor-coordination from 10 weeks of age, followed by progressive ataxia and disease end-stage at 15-16 weeks [28]. All mice were maintained by heterozygous mating. Animal procedures were conducted using protocols approved by the UK Animals (Scientific Procedures) Act (1986).

2.2 Circadian wheel-running screens

Age and sex-matched (7-week old) *Npc1^{nih}* and *Hexb^{-/-}* animals ($n=5-7$ per genotype per behavioural paradigm) with wild-type littermate controls (WT) were housed individually in cages fitted with running wheels (Coulbourn Instruments) maintained at constant temperature and humidity, with *ad libitum* food and water. Up to 6 cages were arranged in light-controlled chambers with externally controlled white LED lighting set at 150 lux at the cage floor level. The behavioural screens that were applied to examine common circadian paradigms are shown in Fig. S1. In the first *Npc1^{nih}* screen (screen 1), animals were entrained to a 12:12 hour light-dark (LD) cycle for 12 days (zeitgeber time (lights on) (ZT)0 = 0600) followed by one-hour light pulse at ZT14. The mice were then placed in constant darkness (DD) for a further 10

days or until mutants reached disease end-stage. In the second *Npc1^{nih}* screen with an independent cohort of animals (screen 2), mice were entrained to a 12:12 hour light-dark (LD) cycle for 12 days (ZT0 = 0600) followed by being subjected to a six-hour phase advance (ZT0 = 0000) and allowed to re-entrain under these conditions up to 10 days. In the *Hexb^{-/-}* screen, mutant and WT littermate mice were entrained to a 12:12 hour light-dark (LD) cycle for 12 days (ZT0 = 0600) followed by one-hour light pulse at ZT14. The mice were then placed in constant darkness (DD) for a further 11 days followed by constant light (150 lux) for 11 days. Data were analysed using Actimetrics Clocklab toolbox for Matlab prior to additional statistical analysis. The circadian period (τ) in LD and DD was quantified by fitting one regression line through 7 consecutive activity onsets. LD data from both *Npc1^{nih}* screens was pooled prior to analysis.

2.3 Passive-Infrared (PIR) sensor screening

PIR sensor-based actigraphy was carried out essentially as previously described [29], with full details expected to be published in the near future (Brown LA *et al.* in preparation). Briefly, mice were singly housed in the same conditions as described above in cages 44 cm long \times 15 cm wide \times 12 cm high with an acrylic block to prevent undetected movement under the food hopper. Raw data from the PIR motion sensors took the form of percentage time active per 10 second epoch, with sensors activated both by gross locomotion and small movements such as turning of the body. A cohort of age- and sex-matched (8.5-week old) *Npc1^{nih}* and WT littermate controls ($n=5$ per genotype) were monitored under a 12:12 LD cycle with white LED illumination at 150 lux.

2.3 Quantitative PCR (RT-qPCR)

Age-matched (7-week old) *Hexb*^{-/-} (*n*=5) and WT littermate controls (*n*=5) were individually housed and entrained to a 12:12 LD cycle at 150 lux for 14 days prior to the day of tissue collection at ZT6. An independent cohort of *Hexb*^{-/-} mutants (*n*=4) and WT littermate controls (*n*=5) were dark-adapted for 48 hours prior to tissue collection to examine the endogenous core clock. Following cervical dislocation, livers were dissected and frozen on dry ice. Brains were immediately sectioned on a steel matrix between bregma 0 and 1 mm posterior. Tissue punches were taken using a 1 mm sample corer (FST Ltd) from the SCN and then snap-frozen. Total RNA was extracted from the SCN and liver tissue using the RNeasyMicro or RNeasyMini kit (Qiagen), respectively. RNA quality was assessed on a 2100 BioAnalyzer using the RNA 6000 Pico Assay (Agilent Technologies) and all samples had RNA integrity (RIN) values over 7.5. SYBR green master mix (Invitrogen) RT-qPCR reactions were run in triplicate on a StepOne Real Time PCR System (Applied Biosystems), with gene expression values calculated using the $2^{-\Delta\Delta C_t}$ calculation and normalised to *Gapdh* expression. Primer sequences and further details of the qPCR products are shown in Table S2.

2.4 Brain pathology

Lipid accumulation in *Hexb*^{-/-} mice was examined in 15 μ m frozen tissue sections stained for Periodic Acid Schiff (PAS), according to the manufacturer's instructions (Sigma). Filipin staining was carried out using a 0.05 mg / ml solution (Sigma) on frozen sections for 2 hours at room temperature and visualised by fluorescent microscopy.

2.5 Retinal histology

Following enucleation whole eyes from *Hexb*^{-/-} mice (*n*=3) and WT littermate controls (*n*=3) were snap frozen on dry ice and stored at -80°C. Eyes were then post fixed in 4% methanol free paraformaldehyde in PBS for 16 hours. Subsequent immunostaining of retina cryostat sections and whole retina flatmounts was performed as described previously [30, 31]. Rabbit polyclonal anti-melanopsin antibody (1:2500, UF006, advanced Targeting Systems) and goat polyclonal anti-Brn3a antibody (1:1000, sc-31985, Santa Cruz Biotech) were incubated overnight (retinal sections) or for 3 days (retina flatmounts) at 4°C in PBS with 0.2% Triton-X and 2% donkey serum. Donkey anti-rabbit Alexa 568 and donkey anti-goat Alexa 488 secondary antibodies diluted in PBS 0.2% Triton-X and 2% donkey serum (1:200) were incubated for 2 hours at 22°C. For staining of retina flatmounts levels of Triton-X were increased to 1%. All wash steps were performed using PBS with 0.05% Tween-20. Samples were mounted in Prolong Gold anti-fade mounting media containing DAPI (Life Technologies).

2.6 Image acquisition

To examine retinal histology fluorescent images were collected using a LSM 710 laser scanning confocal microscope and Zen 2009 image acquisition software (Zeiss). Individual channels were collected sequentially. Laser lines for excitation were 405nm, 488nm and 561nm. Emissions were collected between 440-480, 505-550, and 580-630nm for blue, green and red fluorescence respectively. For all images, global enhancement of brightness and contrast was performed using Zen Lite 2011 image analysis software (Zeiss). Images of retina flatmounts represent maximum intensity projections generated from confocal slices images collected

every 2.5µm, spanning from the ganglion cell layer to the inner plexiform layer. For direct quantitative comparisons all images were acquired and processed under identical conditions.

2.7 Statistics

Statistics for circadian wheel running, qRT-PCR analysis, and immunofluorescence quantification were carried out using GraphPad Prism version 5.0d (GraphPad Software) or SPSS (version 20, IBM). Results are presented as mean ± SEM. All pairwise comparisons were analysed with Bonferroni post-hoc analysis. The effects of genotype and multivariate experiments were analyzed using ANOVA with Bonferroni post-hoc analysis. Differences were considered to be statistically significant at p -values < 0.05.

3. Results

3.1 Circadian behavioural screening

Initially we used home-cage wheel-running to determine the effect of loss-of-function *Npc1* and *Hexb* mutations on several aspects of circadian behavior by comparing *Npc1^{nih}* and *Hexb^{-/-}* mutant mice with their respective WT littermate controls. Due to the rapid, progressive nature of neuropathology in both these models, the wheel-running screens were initiated at 7 weeks of age to limit the influence of the known gait abnormalities on data acquisition [28,32]. In addition, the lengths of the circadian behavioural paradigms themselves were adapted to account for the limited lifespan of these mutants; not all experimental conditions could be tested in an individual mutant. As such, subsequent experimental conditions were chosen based on their phenotype in the initial screen. For example, two independent cohorts of *Npc1^{nih}* mice were required to investigate both entrainment and re-entrainment (see Materials and Methods and Fig. S1 for details of the screens).

Initially we monitored *Npc1^{nih}* mice for their the entrainment to a 12:12 light/dark (LD) cycle (zeitgeber time (ZT)0 = 0600 hrs) (Fig. 1A). *Npc1^{nih}* mice were able to run on the wheels and could entrain to this regular 24-hour lighting schedule, with no significant difference in the time of activity onset, circadian period, or proportion of activity in the light phase compared to their respective WT controls (Fig. 1A-C and Table 1). However, the length of the active phase (alpha) for mutants was significantly shorter compared to WT mice even during the first few days of activity measurements (Fig. 1A and S2A); this demonstrates that wheel-running is able to quantify behavioural alterations prior to the onset of visible ataxia in this model [26].

In addition to the LD entrainment data, we examined negative masking using a one-hour light pulse administered during LD at ZT14 (Fig. S1). All mice tested demonstrated normal negative masking responses to light as shown by suppression of their activity, suggesting light input pathways were functioning normally at 8-9 weeks of age in *Npc1^{ni^h}* mice (Fig. S3). We next investigated free-running activity patterns under constant conditions. Under constant dark (DD), the free-running period (τ) of *Npc1^{ni^h}* mice could be clearly defined from the onset of activity (Fig. 1A); however, this was not significantly different from WT controls (Fig. 1C); these data suggest the core clock is functioning normally in mutant animals. Further examination of wheel-running in *Npc1^{ni^h}* animals over all phases of the circadian screen demonstrated fragmented activity compared to WT mice, as demonstrated by a small increase in the number of activity bouts per day (Fig. S2B). This was accompanied by hypoactivity in *Npc1^{ni^h}* mice, as predicted by their progressive ataxia, with mutants showing a significant reduction in wheel-running under LD and DD; this effect became more pronounced as the mice reached disease end-stage at 10-11 weeks of age (Fig. 1B). Together, these data suggest that *Npc1^{ni^h}* mutants show reduced wheel-running capability but have no overt circadian behavioural abnormalities.

Next we analysed *Hexb^{-/-}* and WT littermate controls under the same circadian parameters of 12:12 LD and DD (Fig. S1). As observed in *Npc1^{ni^h}* mice, *Hexb^{-/-}* mutants displayed entrained 24-hour rest/activity profiles, with no significant difference in the time of activity onset, circadian period, negative masking, or proportion of activity in the light phase compared to WT controls (Fig. 2A-C, Table 2, Fig. S3). *Hexb^{-/-}* mutants displayed a slight reduction in activity in LD compared to

controls, although this was only significant at one particular day in DD (Fig. 2B, Table 2). In contrast to *Npc1^{nih}* mice, the alpha and average number of activity bouts per day in *Hexb^{-/-}* mice was not significantly different to their WT controls (Fig. S2C-D). However, *Hexb^{-/-}* mutants exhibited a small, but statistically significant shorter free-running period (mean tau= 23.3 +/- 0.05 h) versus WT littermates (mean tau= 23.7 +/- 0.06 h; $p = 0.027$) under DD (Fig. 2A and C); this shortened tau suggests that there may be deficits in core clock function in *Hexb^{-/-}* mice.

Hexb^{-/-} mutants display gait abnormalities at a later stage than *Npc1^{nih}* mice, thus we were able to examine free-running behaviour under constant light (LL) in addition to DD in the same circadian screen (Fig. S1). LL is expected to cause a period lengthening effect as a measure of the circadian sensitivity to light and this paradigm was carried out to further investigate the activity onset differences observed in DD. Interestingly, we observed considerable variability in the wheel-running patterns of *Hexb^{-/-}* mutants under LL (Fig. 3A-C). Despite progressive hypoactivity observed in all *Hexb^{-/-}* animals, one third (2 of 6) showed period lengthening as seen in WT mice (Fig. 3A and B), whereas two-thirds of mutants showed a running pattern with a tau value continuing below 24-hours, suggesting light-input pathways are disrupted in these animals towards end-stage disease (Fig. 3C).

Given the potentially fragmented activity in *Npc1^{nih}* mice in DD, next we investigated the ability of the clock to entrain to a new LD cycle in these mutants using a jet-lag or phase-shift paradigm on second cohort of animals (screen 2, Fig. S1); after entrainment to 12:12 LD cycle, a 6-hour phase advance (ZT0 = 0000 hrs) lighting schedule was applied. *Npc1^{nih}* mutants appeared to re-entrain to the new 12:12 LD

cycle, however there was an large additional burst of activity approximately 5 hours prior to lights-off (Fig. 4A). Consequently, there was a significant difference in the average activity onset time after 3 days of the new lighting schedule (Fig. 4B).

We speculated that the differences in activity levels and onset after the jet-lag protocol of *Npc1^{nih}* mutants was due to their progressive, ataxic gait limiting their ability to run, or motivation to run, on the wheel. Therefore we carried out a daily activity screen using an third independent cohort of mice at 8.5 weeks of age using passive-infrared motion sensors [29]. Data were recorded over 5 days under a 12:12 LD cycle (ZT0 = 0600 hrs) in standard homecages lacking a running wheel (Fig. 5A). This method was able to detect stable activity onsets in WT mice at ZT12 with limited activity in the light phase (Fig. 5A). Interestingly, after 2 days of acclimatisation to the cages, these data indicated a significant increase in activity of *Npc1^{nih}* mice towards the second half of the light phase (ZT7-11) compared to WT controls (Fig. 5B); this is a similar pattern of activity to that seen in *Npc1^{nih}* mutants under LD after the phase-advance paradigm (Fig. 4A). However, in the same 24-hour period there was no significant reduction in average activity during the first 6 hours of the dark phase in *Npc1^{nih}* mice (ZT12-18) that would be indicative of a shortened alpha (Fig. 5B). Overall, these data from a short circadian screen using PIR sensors suggest that the reduced alpha observed initially under LD (Fig. S2A) could be due to the influence of the progressive ataxia on wheel-running capability.

3.2 Neuropathology

Although previous studies have demonstrated widespread pathology in the brains of both *Npc1^{nih}* and *Hexb^{-/-}* mice [24,33], we investigated whether the accumulation of

cholesterol and glycosphingolipids occurs specifically in the SCN of *Npc1^{nih}* and *Hexb^{-/-}* mutants, respectively, as this may relate to the differences in wheel-running activity observed under constant conditions. First, PAS staining was used to determine the extent of lipid accumulation in *Hexb^{-/-}* animals in comparison to WT littermates at 12 weeks of age, and strong staining was seen in the hippocampus as reported previously (Fig. 6A-B) [34]. Interestingly, there appeared to be a lack of lipid accumulation in the SCN (Fig. 6C-D). By contrast, in *Npc1^{nih}* mice, extensive cholesterol accumulation was seen in all regions of the brain at 10 weeks of age using filipin staining, including the SCN itself (Fig. 6E-F). These data show that despite obvious pathology in the SCN, *Npc1^{nih}* mutants are still able to maintain a normal circadian phenotype. Thus these data support the hypothesis that the reduced alpha and increased fragmentation observed in these mutants is likely to reflect early markers of disease pathology and ataxia rather than circadian defects.

3.3 Expression analysis

Due to alterations in the free-running activity of *Hexb^{-/-}* mutants, we next investigated the core clock at the molecular level in these mice by measuring the expression of selected clock genes in both the SCN and liver at postnatal day (P)72; a cohort of animals at 8 weeks of age were initially entrained to a 12:12 LD cycle (ZT0 = 0600 hrs) for 14 days before being exposed to DD for 48 hours prior to tissue collection at CT6 to assess expression changes during constant conditions where we observed potential behavioural changes. Quantitative RT-PCR from hypothalamic SCN tissue punches showed no significant changes in the relative expression levels of *Avp*, *Vip*, *Bmal1*, *Per1*, or *Per2* between *Hexb^{-/-}* mutants and WT controls (Fig. 7A). Interestingly, a significant increase in the expression of *Per1* was observed in the

liver of the same *Hexb*^{-/-} mice compared to WT controls under DD (Fig. 7B). To determine whether these expression changes were restricted to constant lighting conditions, a separate cohort of 8-week old animals were subjected to a 12:12 LD cycle for 16 days and tissue as taken at ZT6. Here, a significant increase in *Per1* expression was again observed in the liver (Fig. 7C). These data suggest there is no global disruption of core clock gene expression in *Hexb*^{-/-} mutants.

3.4 Retinal histopathology

The period lengthening effect of LL in *Hexb*^{-/-} mutants suggests there is disruption to the light-input pathways in these animals. To investigate if the retinal ganglion cells (RGCs) mediating circadian responses to light are affected in this model, we assessed the melanopsin-expressing RGCs in *Hexb*^{-/-} mutants. Immunofluorescence was used to compare the expression of the retinal ganglion cell marker Brn3a and the photosensitive retinal ganglion cell (pRGC) photopigment melanopsin in *Hexb*^{-/-} mutants and WT littermate controls. Brn3a was widely expressed in RGCs located in the ganglion cell layer and displaced RGCs present in the inner nuclear layer, but absent from melanopsin expressing photosensitive RGCs (Fig. 8A and B). The anatomy and distribution of melanopsin staining was consistent with previous reports [31]. Multiple distinct subtypes of pRGCs were detected, and overall a significant dorsal ventral gradient in the distribution of pRGCs and levels of melanopsin expression was observed. Although large areas of *Hexb*^{-/-} retina appeared grossly normal, some were found to contain areas of reduced and disrupted Brn3a staining consistent with RGC toxicity and the partial loss of these cells (Fig. 8C), with some showing more significant disruption of Brn3a labelling than others (Fig. S4A). This was typically evident as areas of cell clumping, abnormal cell morphology, and

reduced levels of Brn3a expression. By comparison, levels of melanopsin expression observed in *Hexb*^{-/-} retina was grossly similar to that observed in WT control retina (Fig. S4B). In areas of disrupted Brn3a labelling levels of melanopsin expression and the anatomy of pRGCs was typically normal, although some degree of pRGC disruption was observed in some of the most affected areas. Together, these data suggest that defects in retinal output does not entirely account for the variation in wheel-running towards end-stage in *Hexb*^{-/-} mutants.

4. Discussion

Circadian phenotypes are reported increasingly in neurodegenerative disorders, including LSDs; however, the exact mechanisms linking circadian rhythm disruption and neuropathology remain largely unknown. Here we investigated the effect of mutations in the *Npc1* and *Hexb* genes on the circadian axis in mouse models of NPC1 and Sandhoff disease. Significant insights into the underlying biochemical/molecular basis of LSDs have been gained through the use of animal models [35]. NPC1 (*Npc1^{nih}*) and Sandhoff (*Hexb^{-/-}*) mutant mice recapitulate many features of the corresponding human disorders, including rapid onset of metabolic disease, excessive neuronal storage, and progressive motor and cognitive pathology [24,26,27]. Interestingly, despite some general phenotypic similarities between both mutants, we found some evidence for potential differences in their circadian phenotypes.

Npc1^{nih} mutants showed normal entrainment to a 24-hour LD cycle, and typical free-running circadian periods (tau) under constant dark for the background strain [36], suggesting no overt circadian disruption. However, *Npc1^{nih}* mice did show some re-entrainment deficits following a six-hour LD phase-advance at 9-11 weeks of age; this could be partially attributed to the extensive neuropathology and ataxia near end-stage in these mutants, causing fragmented wheel-running behaviour and apparent hypoactivity [33]. This was partially corroborated by the PIR tracking that also revealed an increase in activity in the light-phase of mutants at the same age under LD. Interestingly, we did not observe clear evidence for a reduction in total activity or shorter alpha in cages without running wheels in our PIR screen,

supporting the notion that the progressive ataxic gait limits the wheel-running capability of *Npc1^{nih}* mutants but not overall activity. A recent study has utilised the same PIR tracking system in parallel with video tracking and wheel-running assays in a mouse model of glutamate receptor dysfunction; these data also demonstrated that specific behavioural rhythms in mutant animals were dependent on the assay used to measure activity [37]. As such, when using running wheels to assay neurological mutants, the confounds of what is a voluntary motor task must be taken into account. Importantly, we were still able to detect robust free-running profiles close to end-stage disease in *Npc1^{nih}* mutants as well as observing activity differences between genotypes from the first few days of screening, illustrating the ability of wheel-running assays to identify novel and subtle behavioural phenotypes [38].

Activity fragmentation was also evident in *Npc1^{nih}* mice as shown by a small but significant increase in the average number of activity bouts per day, which may reflect an underlying defect that gives rise to sleep disturbances or simply represent the requirement to rest between bursts of activity due to ataxia. We also showed extensive cholesterol accumulation in the SCN, however this does not appear to influence the core molecular clock. Yet it has been hypothesised that neuropathology in the brainstem of *Npc1^{nih}* mutants, such as decreased tyrosine-hydroxylase immunoreactivity in locus coeruleus, is indicative of an imbalance between cholinergic and monoaminergic activity, that may in-turn influence non-REM to REM sleep transitions [39]. Interestingly, previous studies report fragmented and disorganised sleep in NPC1 patients [20,21], although further experiments using

telemetry or longer-term video tracking would be required to analyse sleep in LSD models and identify parallels with patients.

We showed that *Hexb*^{-/-} mutants display some evidence for aberrant circadian behaviours, despite an apparent lack of glycosphingolipid accumulation (PAS staining) in the SCN; under the DD paradigm a small but significant reduction in tau was observed, indicative of endogenous clock dysfunction. No differences were seen in the expression of selected core clock genes in the SCN under DD conditions, however. In *Hexb*^{-/-} mice, the pathology is widespread and not simply focussed in the cerebellum, with the cells in the cerebral cortex, thalamus, striatum, hippocampus also showing accumulation of GM2 ganglioside in addition to neuroinflammation and widespread neuronal death [24,34]. Therefore, although it is unclear how the function of these specific brain regions will be affected, it is possible that the widespread nature of the GM2 pathology may lead to circadian feedback to the clock. The differences in *Per1* expression in the *Hexb*^{-/-} liver in both DD and LD could be an indirect result of liver pathology influencing immediate early genes in mutant mice, yet this may also demonstrate uncoupling of peripheral clocks. As clock gene expression appeared normal in the hypothalamus of *Hexb*^{-/-} mice it is unlikely that this could, in turn, feedback to the SCN and influence free-running behaviour. It is becoming increasingly evident, however, that close interaction between central and peripheral clocks is necessary to maintain robust circadian rhythms of physiology and metabolism [40,41].

A range of defective autophagic lysosomal pathways occur in LSDs; from the abnormal enzymatic processing in Sandhoff disease to the non-enzymatic

deficiencies as seen in NPC1 [2,42]. The specific pathways affected result in differential patterns of neurodegeneration, suggesting that specific neuronal subtypes likely contribute to the subtle circadian behavioural changes observed in *Npc1^{nih}* and *Hexb^{-/-}* mice. Previous behavioural studies of other LSD mouse models have also shown contrasting circadian profiles. In a model of mucopolysaccharidosis (MPS) III, mice are deficient for the lysosomal enzyme N-acetyl-glucosaminidase, and lysosomal storage is observed in multiple brain regions including the SCN [43]. These mutants demonstrate a significant increase in activity during the light phase in comparison to controls under a LD cycle, but no free-running deficits [44]. By contrast, mice lacking lysosomal α -mannosidase, a model of the LSD α -mannosidosis were reported to have no circadian abnormalities [45]. Thus it is noteworthy that *Npc1*, *Hexb* and many other genes implicated in LSDs have a fluctuating daily expression profiles at the RNA level [46], suggesting that the biological clock itself may impart additional regulation upon critical lysosomal enzymes and metabolites that will ultimately influence circadian behaviour.

The SCN is innervated by intrinsically photosensitive retinal ganglion cells mediating non-image forming responses to light [47]. Our data show these melanopsin expressing cells showed signs of stress and damage in some areas of the retina in *Hexb^{-/-}* mice. Immunostaining from WT mice showed a pattern of Brn3 and melanopsin staining consistent with previous reports from WT retina [31]. A significant reduction in Brn3a expressing RGCs was observed in the retina of *Hexb^{-/-}* mice in comparison to WT mice. However, these RGCs do not project directly on to the SCN, rather form part of the principal thalamocollicular visual pathway mediating cortical vision [48]. This is in support of previous studies which have illustrated

extensive GM2 deposition in RGCs, vacuolation in retinal neurons, and disruption of the retinal pigment epithelium in *Hexb*^{-/-} mice [49,50,51]. Importantly, these animal studies also correlate with the vision loss identified in Sandhoff disease patients [52]. Previous work has shown that even in the absence of light the eyes still exert effects on circadian behaviour, and key markers of SCN function are unaffected following enucleation [53]. The retinal pathology observed in the *Hexb*^{-/-} mutants may explain the small, but significant, reduction of tau in DD, and explain the lack of core clock gene disruption in the SCN associated with this. Our *Hexb*^{-/-} data suggests mild hypoactivity coupled with end-stage retinal ganglion cell disruption in these mutants. Previous reports suggest the effects of the retinal circadian system on the free-running period is difficult to predict, and it is unknown whether changes observed are a result of the interaction between the retinal and circadian system or due to photoreceptor degeneration [54].

5. Conclusion

The molecular circadian feedback loop regulates the expression of clock-controlled genes in a rhythmic manner, resulting in the oscillation of tissue-specific metabolic and physiological functions [55]. Here we describe two mutant mouse models of LSD that display some minor differences in their circadian behaviour and potential perturbations in the peripheral molecular clock in *Hexb*^{-/-} mutants. Despite the extensive CNS pathology observed in some LSDs, the hypothalamic oscillatory network may remain intact and exhibit only minor defects in these disorders. As we have demonstrated, specific populations of neurons are differentially affected depending on the nature of the disease [56], indicating the alternative mechanisms that underlie the neuropathology in LSDs may influence the rest/activity profiles observed in this group of disorders. More research will be required to understand this relationship and ascertain if the timing of lysosomal enzyme activity could influence therapeutic approaches [46].

Figure legends

Fig. 1: Wheel-running behaviour in *Npc1^{nih}* mutants in LD and DD. (A) *Npc1^{nih}* activity under a 12:12 LD cycle (from 7 weeks of age) followed by DD (*Npc1^{nih}* screen 1; Fig. S1 for details) versus WT controls. Each horizontal line represents a double-plot of the activity profile recorded over 24 hours. Activity bars are displayed in 10 minute bins and yellow shading indicates light exposure. (B) *Npc1^{nih}* mutants show significantly reduced activity over each day in LD ($n=11$ each genotype, *Npc1^{nih}* screens 1 and 2 combined) and DD ($n=5$, *Npc1^{nih}* screen 1) compared to WT controls. (C) Free-running activity onsets do not differ between *Npc1^{nih}* mutants and WT controls ($n=5$, *Npc1^{nih}* screen 1). Data presented as mean \pm SEM; * $p<0.01$, *** $p<0.0001$, ANOVA.

Fig. 2: Wheel-running behaviour in *Hexb^{-/-}* mutants in LD and DD. (A) *Hexb^{-/-}* activity under a 12:12 LD cycle (from 7 weeks of age) followed by DD (*Hexb^{-/-}* screen; Fig. S1 for details) versus WT controls. (B) *Hexb^{-/-}* mutants show no difference in activity over each day in LD and at only one hour during DD ($n=6$, *Hexb* screen 1) compared to WT controls ($n=7$). (C) Free-running activity onsets under DD are significantly earlier in *Hexb^{-/-}* mutants compared to WT. Data presented as mean \pm SEM; * $p<0.05$, ANOVA

Fig. 3: Wheel-running of *Hexb^{-/-}* mutants under constant light (LL). After DD, *Hexb^{-/-}* mutants and controls were placed in LL (Fig. S1; *Hexb^{-/-}* screen). (A and B) One third (2 of 6) of the *Hexb^{-/-}* mutants displayed period lengthening as expected in WT mice.

(C) Two-thirds (4 out of 6) *Hexb*^{-/-} mutants show a photoperiod of less than 24 hours under LL.

Figure 4: Phase-resetting behaviour in *Npc1*^{nih} mutants. (A) *Npc1*^{nih} activity onset following a six-hour phase advance was similar to WT for the first 2 days, however increasing onset variability was observed, indicating rhythm instability (*n*=5). (B) Average activity onsets in *Npc1*^{nih} mice were significantly different from WT 3 days after the phase advance (indicated with an arrow). Data presented as mean ± SEM; **p*<0.01, ****p*<0.0001, ANOVA.

Fig 5: Passive Infrared (PIR) tracking in *Npc1*^{nih} mutants in a 12:12 LD cycle. Each row represents a double-plot of the activity profile recorded over 24 hours. (A) Activity bars are displayed in 10 minute bins and yellow shading indicates light exposure. (B) Average activity over day 3 of the PIR screen. *Npc1*^{nih} mutants show significant increase in light-phase activity compared to WT. ***p*<0.01, ****p*<0.0001.

Fig. 6: Neuropathology of LSD mouse models. (A-D) Representative light microscopy images of Periodic Acid–Schiff (PAS)-stained brain sections from *Hexb*^{-/-} mutants and WT controls at 12 weeks of age. Stained sections are taken from the dentate gyrus (A, B) and the SCN (C, D). The glycosphingolipid (GSL) storage products stained with PAS appear pink. Arrows indicate PAS-positive neuronal inclusions in *Hexb*^{-/-} mutants. (E, F) Representative fluorescent microscopy images of filipin-stained SCN sections from *Npc1*^{nih} mutant and WT controls at 11 weeks of age. Scale bars: 100µm.

Fig. 7: Clock gene expression in *Hexb*^{-/-} mutants by qRT-PCR. (A) No significant difference in selected clock gene expression was observed in the SCN of *Hexb*^{-/-} mutants versus WT at CT6 under DD (*n*=4-5). *Hexb*^{-/-} mutants show a significant differences in the expression of *Per1* in the liver at ZT6 under a 12:12 LD cycle (B) and at CT6 under DD compared (C) to WT (*n*=4-5). Data are presented as mean ± SEM; **p*<0.001, ANOVA.

Fig. 8: Retinal histopathology in *Hexb*^{-/-} mutants. (A) Representative immunofluorescence images of Brn3a and melanopsin expression in WT ventral retina (*n*=3). (B) Representative immunofluorescence images of Brn3a and melanopsin expression in *Hexb*^{-/-} ventral retina (*n*=3). (C) Some dorsal areas of *Hexb*^{-/-} retina showed more significant disruption of Brn3a labelling. Scale bars: 50µm.

Table 1: Circadian activity parameters for *Npc1*^{nih} mice during LD and LL

Table 2: Circadian activity parameters for *Hexb*^{-/-} mice during LD

Acknowledgements

The research leading to these results has received funding from the European Union Seventh Framework Programme (FP7/2007-2013) under grant agreement number 311394 to P.L.O. and a UK Medical Research Council Programme Grant to K.E.D.

References

- [1] Fuller PM, Gooley JJ, Saper CB. Neurobiology of the sleep-wake cycle: sleep architecture, circadian regulation, and regulatory feedback. *Journal of biological rhythms*. 2006;21:482-93.
- [2] Platt FM, Boland B, van der Spoel AC. The cell biology of disease: lysosomal storage disorders: the cellular impact of lysosomal dysfunction. *The Journal of cell biology*. 2012;199:723-34.
- [3] Futerman AH, van Meer G. The cell biology of lysosomal storage disorders. *Nature reviews Molecular cell biology*. 2004;5:554-65.
- [4] Saftig P, Klumperman J. Lysosome biogenesis and lysosomal membrane proteins: trafficking meets function. *Nature reviews Molecular cell biology*. 2009;10:623-35.
- [5] Kwon HJ, Abi-Mosleh L, Wang ML, Deisenhofer J, Goldstein JL, Brown MS, et al. Structure of N-terminal domain of NPC1 reveals distinct subdomains for binding and transfer of cholesterol. *Cell*. 2009;137:1213-24.
- [6] Vanier MT. Niemann-Pick disease type C. *Orphanet journal of rare diseases*. 2010;5:16.
- [7] Vance JE, Karten B. Niemann-Pick C disease and mobilization of lysosomal cholesterol by cyclodextrin. *Journal of lipid research*. 2014;55:1609-21.
- [8] Staretz-Chacham O, Lang TC, LaMarca ME, Krasnewich D, Sidransky E. Lysosomal storage disorders in the newborn. *Pediatrics*. 2009;123:1191-207.
- [9] Wulff K, Gatti S, Wettstein JG, Foster RG. Sleep and circadian rhythm disruption in psychiatric and neurodegenerative disease. *Nature reviews Neuroscience*. 2010;11:589-99.

- [10] Musiek ES, Xiong DD, Holtzman DM. Sleep, circadian rhythms, and the pathogenesis of Alzheimer disease. *Experimental & molecular medicine*. 2015;47:e148.
- [11] Goodman AO, Rogers L, Pilsworth S, McAllister CJ, Shneerson JM, Morton AJ, et al. Asymptomatic sleep abnormalities are a common early feature in patients with Huntington's disease. *Current neurology and neuroscience reports*. 2011;11:211-7.
- [12] Postuma RB, Gagnon JF, Vendette M, Fantini ML, Massicotte-Marquez J, Montplaisir J. Quantifying the risk of neurodegenerative disease in idiopathic REM sleep behavior disorder. *Neurology*. 2009;72:1296-300.
- [13] Romenets SR, Gagnon JF, Latreille V, Panniset M, Chouinard S, Montplaisir J, et al. Rapid eye movement sleep behavior disorder and subtypes of Parkinson's disease. *Movement disorders : official journal of the Movement Disorder Society*. 2012;27:996-1003.
- [14] Colville GA, Watters JP, Yule W, Bax M. Sleep problems in children with Sanfilippo syndrome. *Developmental medicine and child neurology*. 1996;38:538-44.
- [15] Kirveskari E, Partinen M, Santavuori P. Sleep and its disturbance in a variant form of late infantile neuronal ceroid lipofuscinosis (CLN5). *Journal of child neurology*. 2001;16:707-13.
- [16] Fraser J, Gason AA, Wraith JE, Delatycki MB. Sleep disturbance in Sanfilippo syndrome: a parental questionnaire study. *Archives of disease in childhood*. 2005;90:1239-42.
- [17] Hendriksz CJ, Corry PC, Wraith JE, Besley GT, Cooper A, Ferrie CD. Juvenile Sandhoff disease--nine new cases and a review of the literature. *Journal of inherited metabolic disease*. 2004;27:241-9.

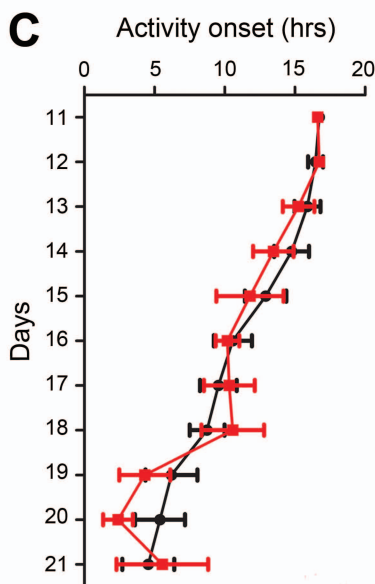
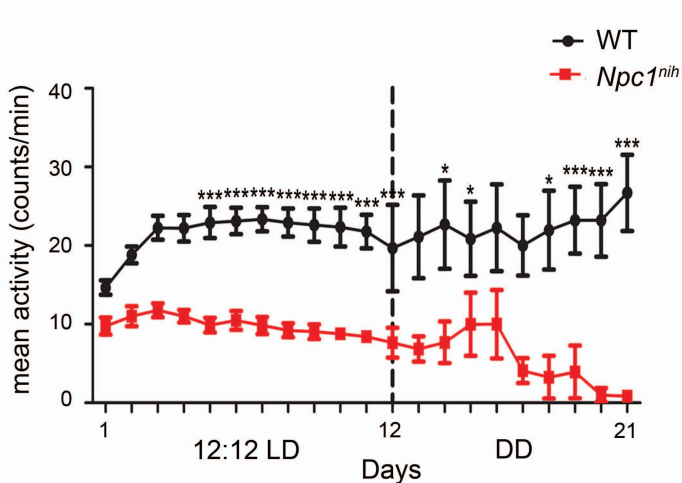
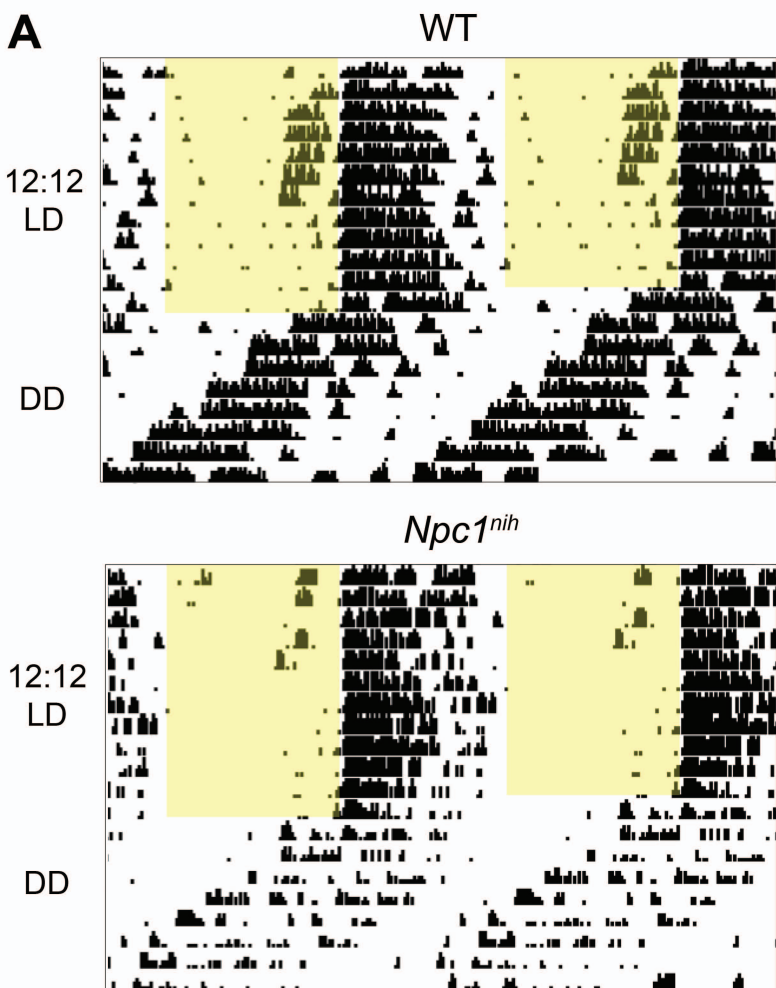
- [18] Maegawa GH, Stockley T, Tropak M, Banwell B, Blaser S, Kok F, et al. The natural history of juvenile or subacute GM2 gangliosidosis: 21 new cases and literature review of 134 previously reported. *Pediatrics*. 2006;118:e1550-62.
- [19] Kanbayashi T, Abe M, Fujimoto S, Miyachi T, Takahashi T, Yano T, et al. Hypocretin deficiency in niemann-pick type C with cataplexy. *Neuropediatrics*. 2003;34:52-3.
- [20] Vankova J, Stepanova I, Jech R, Elleder M, Ling L, Mignot E, et al. Sleep disturbances and hypocretin deficiency in Niemann-Pick disease type C. *Sleep*. 2003;26:427-30.
- [21] Nevsimalova S, Malinova V. Cataplexy and sleep disorders in Niemann-Pick type C disease. *Current neurology and neuroscience reports*. 2015;15:522.
- [22] Turek FW, Joshu C, Kohsaka A, Lin E, Ivanova G, McDearmon E, et al. Obesity and metabolic syndrome in circadian Clock mutant mice. *Science*. 2005;308:1043-5.
- [23] Bechtold DA, Brown TM, Luckman SM, Piggins HD. Metabolic rhythm abnormalities in mice lacking VIP-VPAC2 signaling. *American journal of physiology Regulatory, integrative and comparative physiology*. 2008;294:R344-51.
- [24] Phaneuf D, Wakamatsu N, Huang JQ, Borowski A, Peterson AC, Fortunato SR, et al. Dramatically different phenotypes in mouse models of human Tay-Sachs and Sandhoff diseases. *Human molecular genetics*. 1996;5:1-14.
- [25] Loftus SK, Morris JA, Carstea ED, Gu JZ, Cummings C, Brown A, et al. Murine model of Niemann-Pick C disease: mutation in a cholesterol homeostasis gene. *Science*. 1997;277:232-5.
- [26] Voikar V, Rauvala H, Ikonen E. Cognitive deficit and development of motor impairment in a mouse model of Niemann-Pick type C disease. *Behavioural brain research*. 2002;132:1-10.

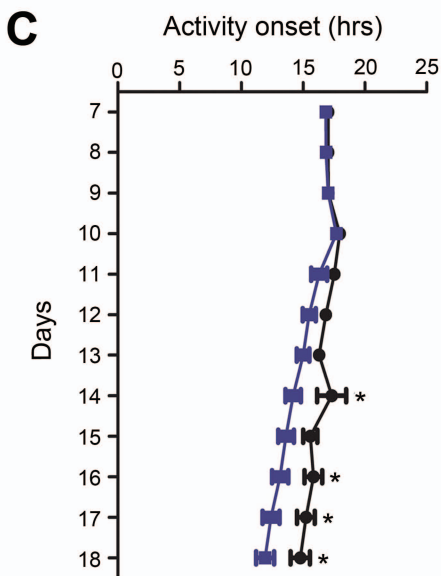
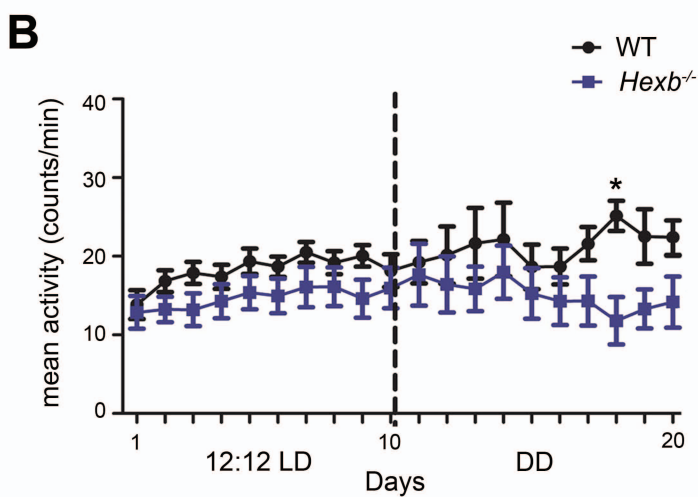
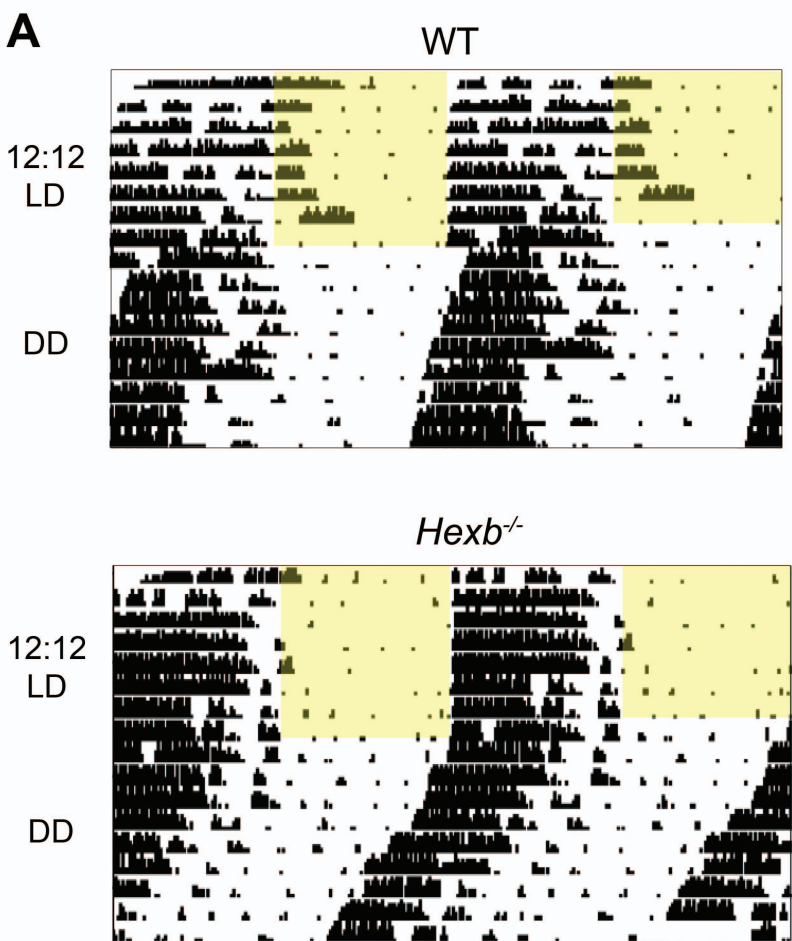
- [27] Baudry M, Yao Y, Simmons D, Liu J, Bi X. Postnatal development of inflammation in a murine model of Niemann-Pick type C disease: immunohistochemical observations of microglia and astroglia. *Experimental neurology*. 2003;184:887-903.
- [28] Sango K, Yamanaka S, Hoffmann A, Okuda Y, Grinberg A, Westphal H, et al. Mouse models of Tay-Sachs and Sandhoff diseases differ in neurologic phenotype and ganglioside metabolism. *Nature genetics*. 1995;11:170-6.
- [29] Pritchett D, Jagannath A, Brown LA, Tam SK, Hasan S, Gatti S, et al. Deletion of Metabotropic Glutamate Receptors 2 and 3 (mGlu2 & mGlu3) in Mice Disrupts Sleep and Wheel-Running Activity, and Increases the Sensitivity of the Circadian System to Light. *PloS one*. 2015;10:e0125523.
- [30] Hughes S, Pothecary CA, Jagannath A, Foster RG, Hankins MW, Peirson SN. Profound defects in pupillary responses to light in TRPM-channel null mice: a role for TRPM channels in non-image-forming photoreception. *The European journal of neuroscience*. 2012;35:34-43.
- [31] Hughes S, Watson TS, Foster RG, Peirson SN, Hankins MW. Nonuniform distribution and spectral tuning of photosensitive retinal ganglion cells of the mouse retina. *Current biology : CB*. 2013;23:1696-701.
- [32] Maue RA, Burgess RW, Wang B, Wooley CM, Seburn KL, Vanier MT, et al. A novel mouse model of Niemann-Pick type C disease carrying a D1005G-Npc1 mutation comparable to commonly observed human mutations. *Human molecular genetics*. 2012;21:730-50.
- [33] Pressey SN, Smith DA, Wong AM, Platt FM, Cooper JD. Early glial activation, synaptic changes and axonal pathology in the thalamocortical system of Niemann-Pick type C1 mice. *Neurobiology of disease*. 2012;45:1086-100.

- [34] Jeyakumar M, Thomas R, Elliot-Smith E, Smith DA, van der Spoel AC, d'Azzo A, et al. Central nervous system inflammation is a hallmark of pathogenesis in mouse models of GM1 and GM2 gangliosidosis. *Brain : a journal of neurology*. 2003;126:974-87.
- [35] Pastores GM, Torres PA, Zeng BJ. Animal models for lysosomal storage disorders. *Biochemistry Biokhimiia*. 2013;78:721-5.
- [36] Schwartz WJ, Zimmerman P. Circadian timekeeping in BALB/c and C57BL/6 inbred mouse strains. *The Journal of neuroscience : the official journal of the Society for Neuroscience*. 1990;10:3685-94.
- [37] Pritchett D, Hasan S, Tam SK, Engle SJ, Brandon NJ, Sharp T, et al. d-amino acid oxidase knockout (Dao^{-/-}) mice show enhanced short-term memory performance and heightened anxiety, but no sleep or circadian rhythm disruption. *The European journal of neuroscience*. 2015;41:1167-79.
- [38] Bacon Y, Ooi A, Kerr S, Shaw-Andrews L, Winchester L, Breeds S, et al. Screening for novel ENU-induced rhythm, entrainment and activity mutants. *Genes, brain, and behavior*. 2004;3:196-205.
- [39] Luan Z, Saito Y, Miyata H, Ohama E, Ninomiya H, Ohno K. Brainstem neuropathology in a mouse model of Niemann-Pick disease type C. *Journal of the neurological sciences*. 2008;268:108-16.
- [40] Peek CB, Ramsey KM, Marcheva B, Bass J. Nutrient sensing and the circadian clock. *Trends in endocrinology and metabolism: TEM*. 2012;23:312-8.
- [41] Tsang AH, Barclay JL, Oster H. Interactions between endocrine and circadian systems. *Journal of molecular endocrinology*. 2014;52:R1-16.
- [42] Schulze H, Sandhoff K. Lysosomal lipid storage diseases. *Cold Spring Harbor perspectives in biology*. 2011;3.

- [43] Wilkinson FL, Holley RJ, Langford-Smith KJ, Badrinath S, Liao A, Langford-Smith A, et al. Neuropathology in mouse models of mucopolysaccharidosis type I, IIIA and IIIB. *PloS one*. 2012;7:e35787.
- [44] Canal MM, Wilkinson FL, Cooper JD, Wraith JE, Wynn R, Bigger BW. Circadian rhythm and suprachiasmatic nucleus alterations in the mouse model of mucopolysaccharidosis IIIB. *Behavioural brain research*. 2010;209:212-20.
- [45] D'Hooge R, Lullmann-Rauch R, Beckers T, Balschun D, Schwake M, Reiss K, et al. Neurocognitive and psychotiform behavioral alterations and enhanced hippocampal long-term potentiation in transgenic mice displaying neuropathological features of human alpha-mannosidosis. *The Journal of neuroscience : the official journal of the Society for Neuroscience*. 2005;25:6539-49.
- [46] Mazzocchi G, Mazza T, Vinciguerra M, Castellana S, Scarpa M. The biological clock and the molecular basis of lysosomal storage diseases. *JIMD reports*. 2015;18:93-105.
- [47] Hattar S, Liao HW, Takao M, Berson DM, Yau KW. Melanopsin-containing retinal ganglion cells: architecture, projections, and intrinsic photosensitivity. *Science*. 2002;295:1065-70.
- [48] Quina LA, Pak W, Lanier J, Banwait P, Gratwick K, Liu Y, et al. Brn3a-expressing retinal ganglion cells project specifically to thalamocortical and collicular visual pathways. *The Journal of neuroscience : the official journal of the Society for Neuroscience*. 2005;25:11595-604.
- [49] Sango K, Takano M, Ajiki K, Tokashiki A, Arai N, Kawano H, et al. Impaired neurite outgrowth in the retina of a murine model of Sandhoff disease. *Investigative ophthalmology & visual science*. 2005;46:3420-5.

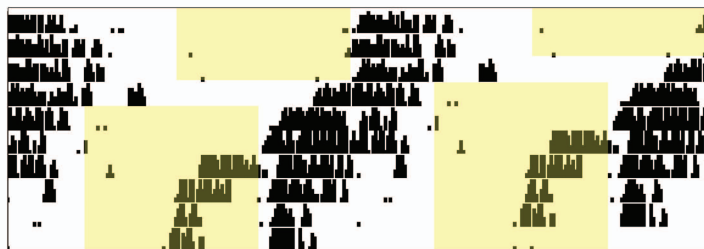
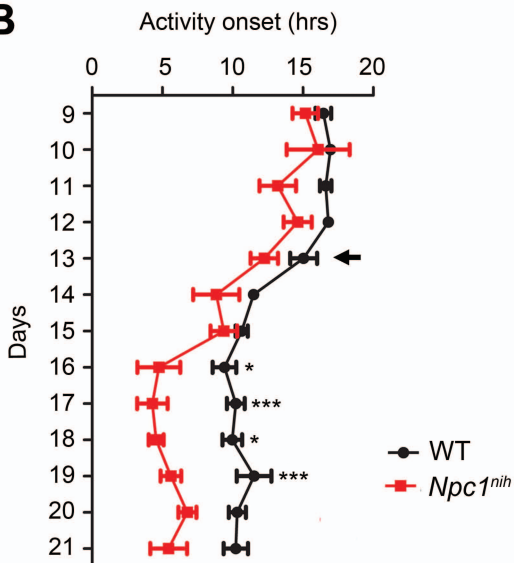
- [50] Sango K, Yamanaka S, Ajiki K, Arai N, Takano M. Involvement of retinal neurons and pigment epithelial cells in a murine model of sandhoff disease. *Ophthalmic research*. 2008;40:241-8.
- [51] Denny CA, Alroy J, Pawlyk BS, Sandberg MA, d'Azzo A, Seyfried TN. Neurochemical, morphological, and neurophysiological abnormalities in retinas of Sandhoff and GM1 gangliosidosis mice. *Journal of neurochemistry*. 2007;101:1294-302.
- [52] Brownstein S, Carpenter S, Polomeno RC, Little JM. Sandhoff's disease (GM2 gangliosidosis type 2). Histopathology and ultrastructure of the eye. *Arch Ophthalmol*. 1980;98:1089-97.
- [53] Yamazaki S, Alones V, Menaker M. Interaction of the retina with suprachiasmatic pacemakers in the control of circadian behavior. *Journal of biological rhythms*. 2002;17:315-29.
- [54] Panda S, Provencio I, Tu DC, Pires SS, Rollag MD, Castrucci AM, et al. Melanopsin is required for non-image-forming photic responses in blind mice. *Science*. 2003;301:525-7.
- [55] Yoo SH, Yamazaki S, Lowrey PL, Shimomura K, Ko CH, Buhr ED, et al. PERIOD2::LUCIFERASE real-time reporting of circadian dynamics reveals persistent circadian oscillations in mouse peripheral tissues. *Proceedings of the National Academy of Sciences of the United States of America*. 2004;101:5339-46.
- [56] Parente MK, Rozen R, Cearley CN, Wolfe JH. Dysregulation of gene expression in a lysosomal storage disease varies between brain regions implicating unexpected mechanisms of neuropathology. *PloS one*. 2012;7:e32419.

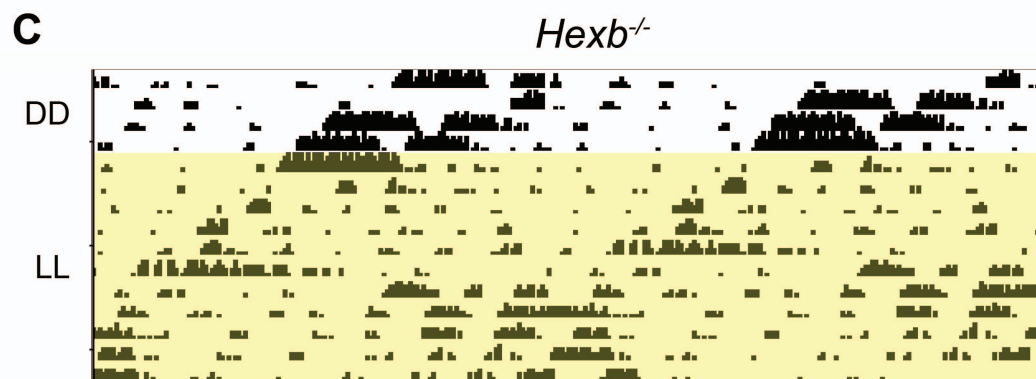
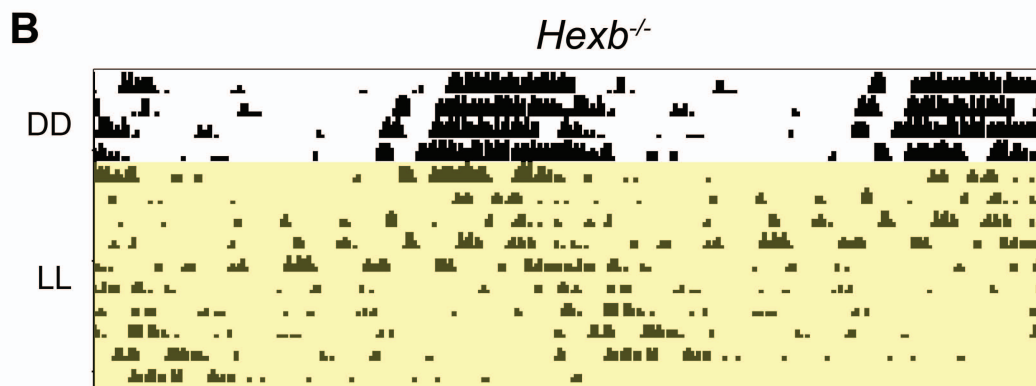
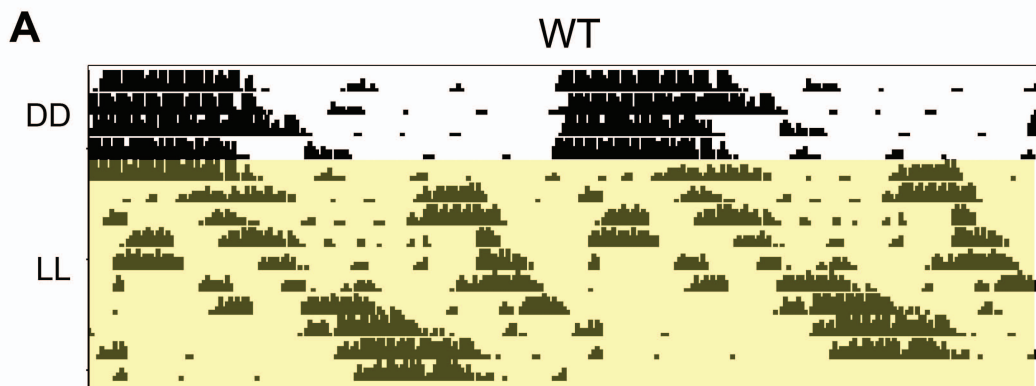




A

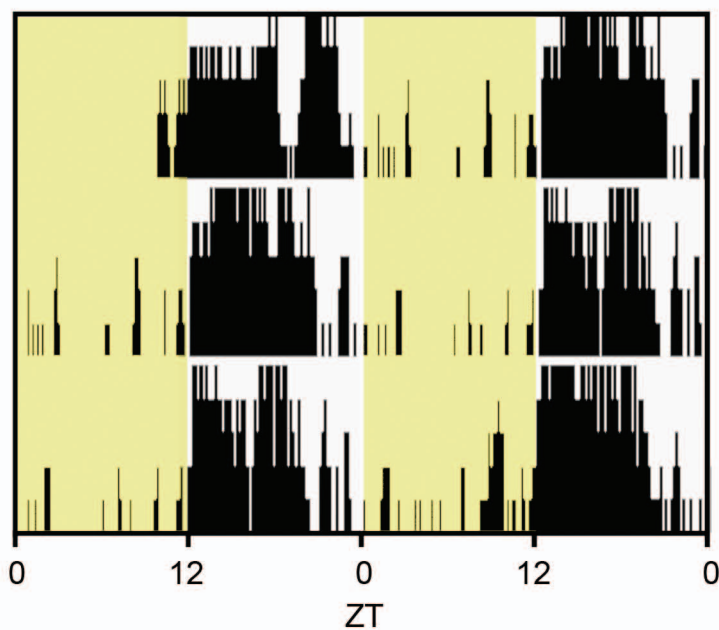
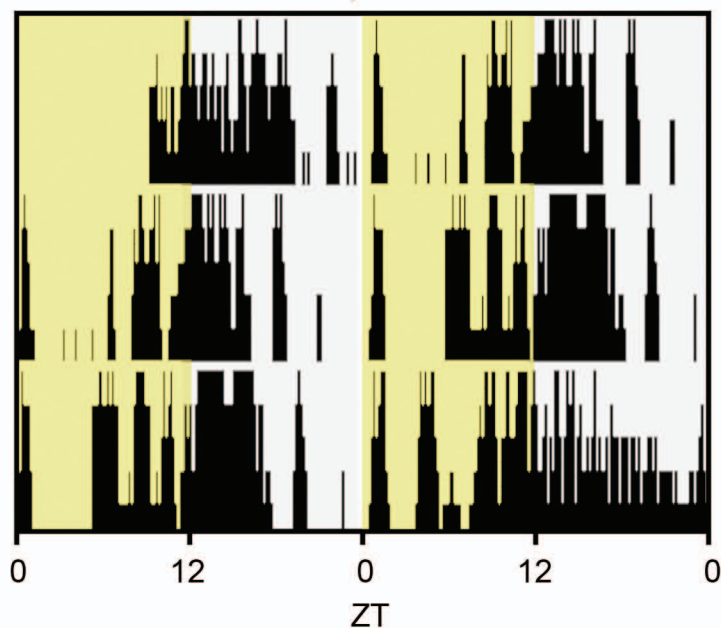
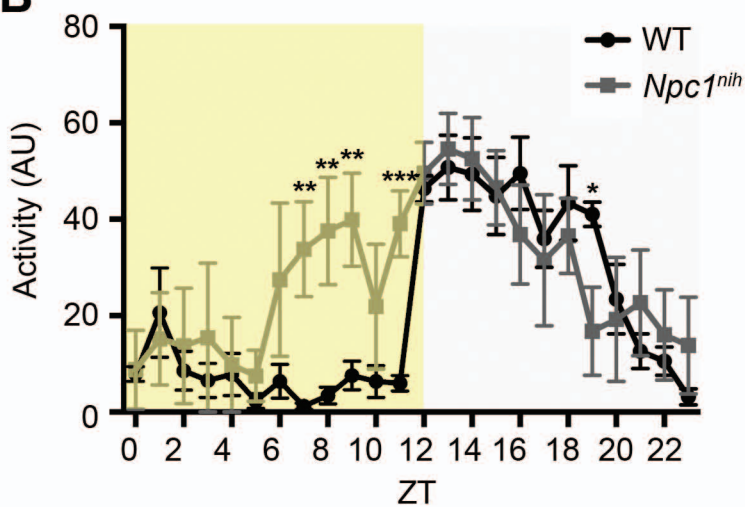
WT

*Npc1^{nih}***B**



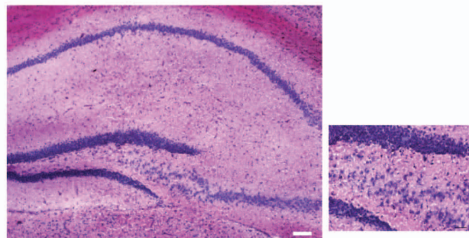
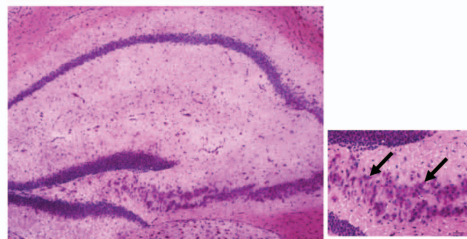
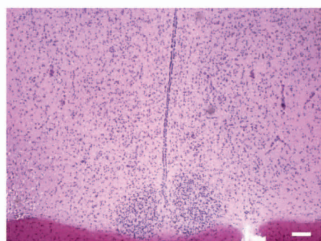
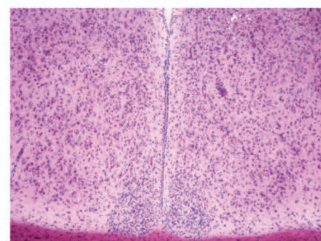
A

WT

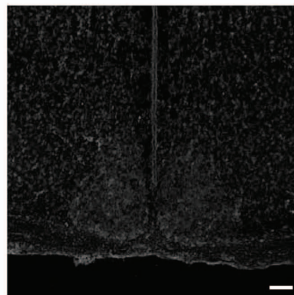
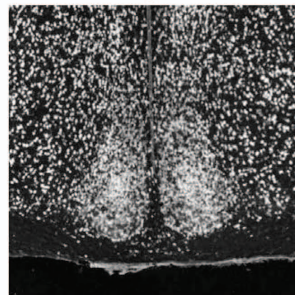
*Npc1^{nih}***B**

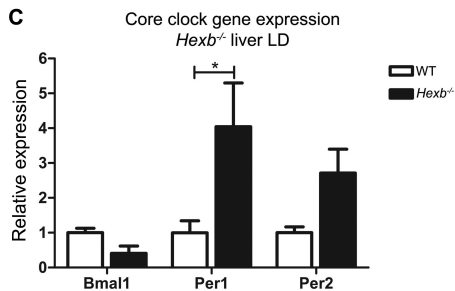
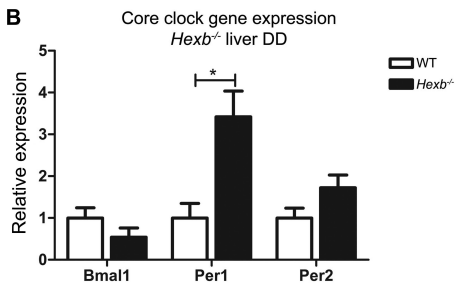
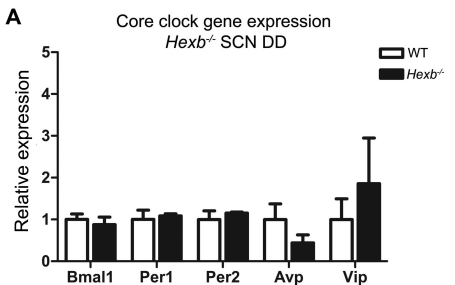
A

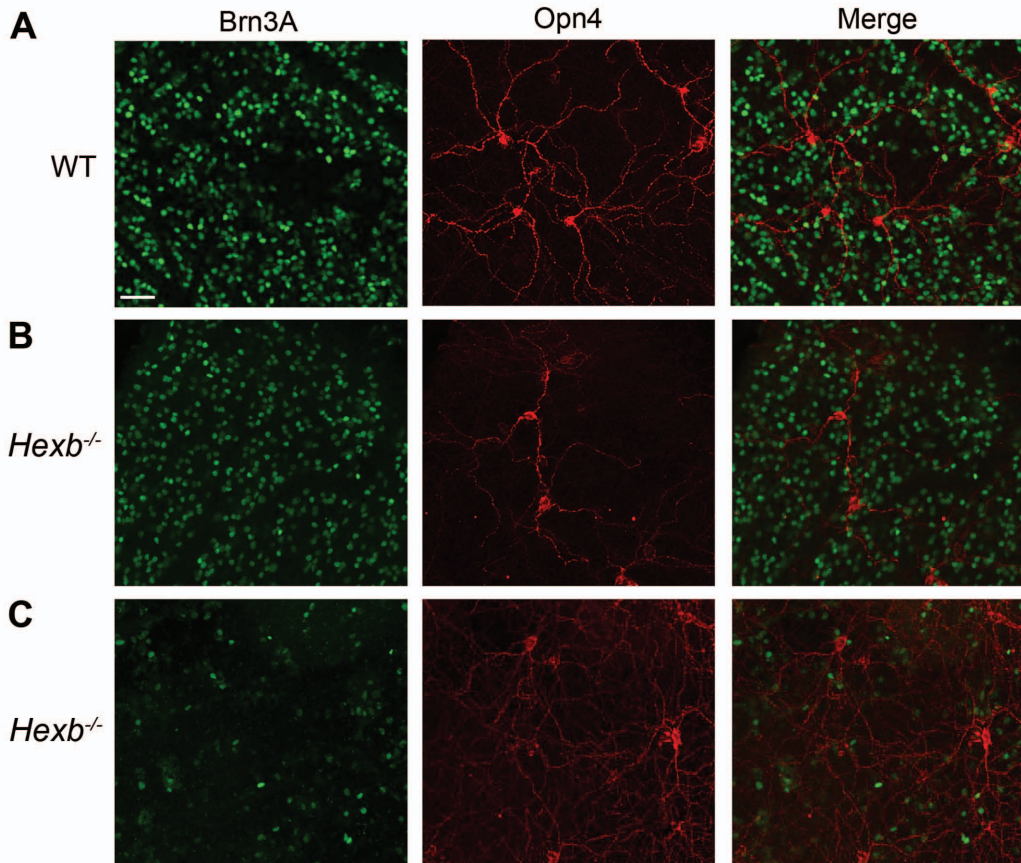
WT

**B***Hexb*^{-/-}**C****D****E**

WT

**F***Npc*^{nih}





Parameter	WT Mean (\pm SEM)	<i>Npc1^{nih}</i> Mean (\pm SEM)	Significance
Activity Onset (hrs)	16.1 (0.23)	15.6 (0.38)	NS
Light activity	12.34 (2.167)	16.59 (3.196)	NS
Circadian period	24.05 (0.05)	24.04 (0.07)	NS
Total activity counts/day	31083 (2033)	14178 (1051)	< 0.0001

Table 1: Circadian activity parameters for *Npc1^{nih}* mice during LD

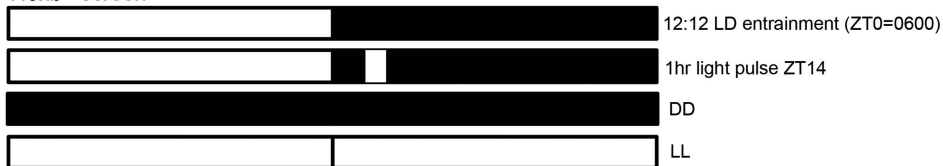
Parameter	WT Mean (±SEM)	<i>Hexb</i> ^{-/-} Mean (±SEM)	Significance
Activity Onset (hrs)	17.10 (0.04)	16.92 (0.05)	NS
Light activity	8.185 (3.40)	3.319 (1.12)	NS
Circadian period	23.84 (0.04)	23.95 (0.02)	NS
Total activity counts/day	25767 (1312)	20847 (2939)	NS

Table 2: Circadian activity parameters for *Hexb*^{-/-} mice during LD

A *Npc^{nih}* screen 1

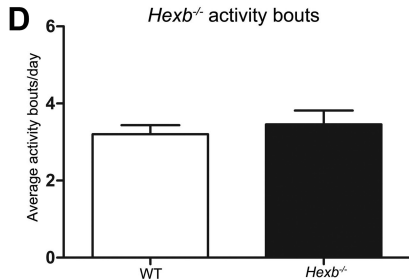
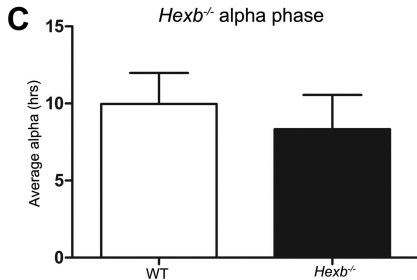
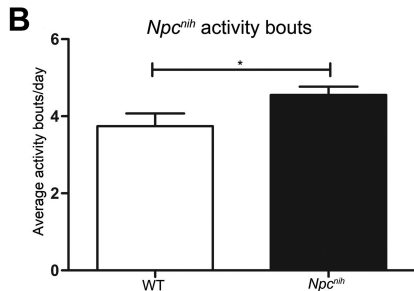
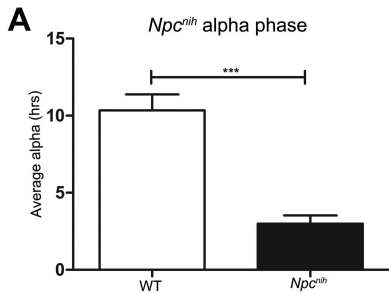


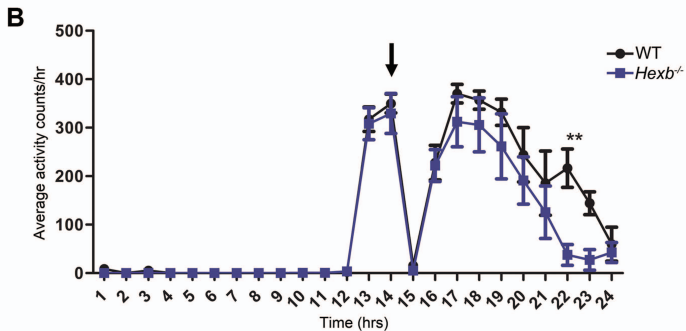
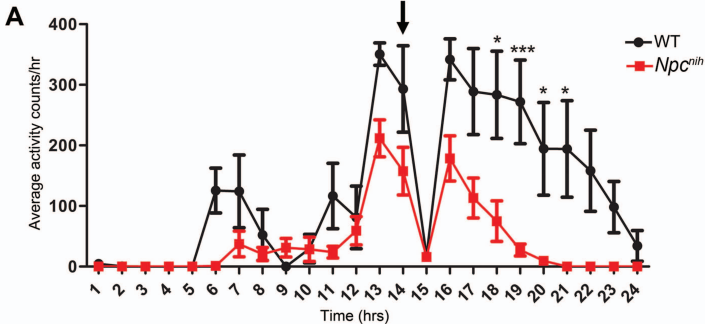
B *Hexb^{-/-}* screen

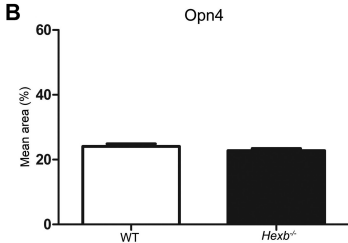
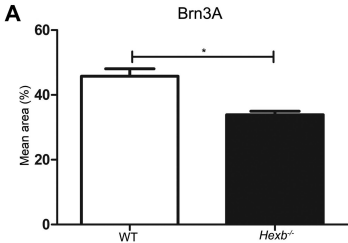


C *Npc^{nih}* screen 2









Parameter	WT Mean (\pm SEM)	<i>Npc1^{nh}</i> Mean (\pm SEM)	Significance
-----------	----------------------	--	--------------

Primer	5'-primer (5'-3')	3'-primer (5'-3')	Annealing temperature (°C)	Product length
Gapdh:	TGTGTCCGTCGTGGATC TGA	CCTGCTTCACCACCTTCT TG	68	77
Per1	GGGTGAGATTCGTCATT GAACTTG	AGGACATTGGCACACTG GAAAGAG	68	119
Bmal1	GAGGTGCCACCAACCCA TAC	AGTCAAACAAGCTCTGG CCAA	67	207
Per2	CCAGGATGTGGGTGTCT TCT	GAGACCTGAACCTGCAG AGG	64.0	85

Avp	CAGGATGCTCAACACTACGC	CTCTTGGGCAGTTCTGGAAG	68	82
Vip	TTTCACCAGCGATTACAGCAG	GCTGATTCGTTTGCCAATGAG	68	86

Supplementary Figure legends:

Fig. S1: Circadian wheel-running screens used in this study. (A) *Npc1^{nih}* circadian screen 1. (B) *Hexb^{-/-}* circadian screen. (C) *Npc1^{nih}* circadian screen 2. The Zeitgeber time (ZT) of all environmental lighting changes is indicated. DD: constant dark, LL: constant light. LD: light/dark.

Fig. S2: Wheel-running activity measurements. (A) *Npc1^{nih}* mice demonstrated a shorter active phase (alpha) compared to WT mice, accompanied by an increase in the number of activity bouts per day during LD (B) ($n=11$). (C, D) No significant differences were observed in the length of the active phase or the number of bouts in *Hexb^{-/-}* mice versus controls ($n=7$). Data are presented as mean \pm SEM; * $p<0.05$, *** $p<0.001$, Student's t-test.

Fig. S3: Negative masking. Average activity counts are shown under 12:12 LD over a 24-hour period with lights off at ZT12. Both *Npc^{nih}* (A) and *Hexb^{-/-}* mice (B) at 8-9 weeks of age displayed a normal suppression of activity in response to a 1 hour light pulse given at ZT14 (arrow). Hypoactivity in the dark phase is also observed in both mutants. Data presented as mean \pm SEM; * $p<0.05$, ** $p<0.01$, *** $p<0.0001$, two-way ANOVA.

Fig. S4: Retinal histopathology. (A) Quantification of Brn3a expression in WT and *Hexb^{-/-}* retina ($n=3$). (B) Quantification of Opn4 expression in WT and *Hexb^{-/-}* retina ($n=3$). Data values represent the percentage area of each confocal image showing positive immunostaining above background. Values were calculated by performing

automated threshold analysis followed by measurement of area above threshold using standard setting in Image J (NIH). Analysis performed on $n=26$ images ($HexB^{-/-}$) and $n=14$ images (WT) collected from $n=3$ retina for each group. Data presented as mean \pm SEM; *** $p<0.001$, Student's t-test.